MOX–Report No. 12/2010

A multiphysics/multiscale numerical simulation of scaffold-based cartilage regeneration under interstitial perfusion in a bioreactor

Riccardo Sacco, Paola Causin, Paolo Zunino, Manuela T. Raimondi

MOX, Dipartimento di Matematica "F. Brioschi"
Politecnico di Milano, Via Bonardi 9 - 20133 Milano (Italy)

mox@mate.polimi.it http://mox.polimi.it

A multiphysics/multiscale numerical simulation of scaffold-based cartilage regeneration under interstitial perfusion in a bioreactor *

Riccardo Sacco[◇], Paola Causin[⋆], Paolo Zunino[♯], Manuela T. Raimondi[†]

April 7, 2010

[◇]Dipartimento di Matematica "F. Brioschi", Politecnico di Milano
Piazza Leonardo da Vinci 32, 20133 Milano, Italy
riccardo.sacco@polimi.it

[⋆]Dipartimento di Matematica "L. Enriques", Università degli Studi di Milano
via Saldini 50, 20133 Milano, Italy
paola.causin@unimi.it

[♯]MOX - Modellistica e Calcolo Scientifico
Dipartimento di Matematica "F. Brioschi', Politecnico di Milano
Piazza Leonardo da Vinci 32, 20133 Milano, Italy
paolo.zunino@polimi.it

[†]LaBS - Laboratory of Biological Structure Mechanics,
Dipartimento di Ingegneria Strutturale, Politecnico di Milano
Piazza Leonardo da Vinci 32, 20133 Milano, Italy
and IRCCS Galeazzi Orthopaedic Institute, Milano, Italy
manuela.raimondi@polimi.it

Keywords: Tissue engineering, Artificial cartilage. Computational model, Multiphysics, Multiscale, Interstitial Perfusion, Bioreactor, Fluid dynamics, Transport, Shear stress

Abstract

Articular cartilage is a connective tissue consisting of a relatively few number of cells, the chondrocytes (CCs), that are immersed in an extensive hydrated matrix, composed primarily of proteoglycans and collagens.

*The Author PC was supported by the Italian Research Funding Program PRIN 2007 "Modellistica numerica per il calcolo scientifico ed applicazioni avanzate". The Author PZ was supported by the European Research Council Advanced Grant "Mathcard, Mathematical Modelling and Simulation of the Cardiovascular System", Project ERC-2008-AdG 227058.

In vitro tissue engineering has been investigated as a potential source of functional tissue constructs for cartilage repair, as well as a model system for controlled studies of cartilage development and function. Among the different kinds of devices for the cultivation of 3D cartilage cell colonies, we consider here polymeric scaffold-based perfusion bioreactors. The perfusion fluid supplies nutrients and oxygen to the growing biomass. At the same time, the fluid-induced shear acts as a physiologically relevant stimulus for the metabolic activity of CCs, because it may enhance cell proliferation and metabolism, provided that the shear stress level is moderate. In this complex environment, mathematical and computational modeling may help in the optimal design of the bioreactor configuration. In this perspective, we propose a computational model for the simulation of the biomass growth, under given inlet and geometrical conditions. Precisely, we consider a two-step approach. First, we perform a simplified short term analysis in which only biomass growth is taken into account, the nutrient concentration and the fluid-induced shear stress being assumed constant in time and uniform in space. This allows us to calibrate the biomass growth model with respect to the shear stress dependence on experimental data. Then, we carry out a full analysis where the nutrient concentration and perfusion velocity change in time and space and the growing biomass modifies the porosity of the scaffold matrix, altering the fluid flow. The model parameters are consistently derived from volume averaging techniques that allow us to upscale the microscopic structural properties to the macroscopic level. The predictions we obtain in this way are significant for long times of culture.

1 Introduction

A basic concept in the design of *ex vivo* tissue reconstruction is to provide a proper biophysical microenvironment to cells [28, 21, 37]. In scaffold-based cartilage regeneration, a procedure for tissue growth based on interstitial flow of the culture medium, also called "direct" or "confined" perfusion, is found to be particularly effective, compared both to static culture and to surface (or "free flow") perfusion, in preserving cell viability, promoting cell proliferation and upregulating the synthesis of matrix proteins specific to cartilaginous tissue, such as collagens and glycosaminoglycan (GAG) [11, 30, 10, 34, 35, 14]. These beneficial effects are primarily related to an improved cell oxygenation and catabolite removal induced by interstitial convective flow in the internal regions of densely cell-populated constructs. Perfusion flow also exerts shear stresses on the cell surface, causing membrane stretch [12, 20]; this mechanism, far from being just a side effect, is recognized to activate specific signalling pathways in articular cartilage cells, which in turn may stimulate cell proliferation and/or enhance cell metabolism, provided that the shear stress level is appropriately tuned [19, 40]. As a matter of fact, increasing the hydrodynamic shear level in cellular constructs is recognized to inhibit the synthesis of sulphated GAG (sGAG) [33] and of collagen type II [36], which are phenotypic markers of articular cartilage. The above considerations suggest that an efficient bioreactor should be

able to provide the growing cells with the highest oxygenation level compatible with a moderate fluid-mechanical loading. Achieving such a balance is a difficult task, since there is a nonlinear interplay between the biophysical conditions experienced at the microscopic pore scale and at the subcellular scale and the macroscopic project parameters of the bioreactor, for example the fluid velocity gradient across the bioreactor thickness or the pressure drop, which are directly related to input control parameters of the system (in our case, the inlet velocity of the perfusion fluid). Furthermore, when designing a bioreactor, one must also face the difficulty that measurements -to name one, the shear stress levels in the growing biomass- cannot be easily accessible and data elaboration does not often allow to draw a clear rationale of the phenomena leading to an optimal design. In this scenario, mathematical and computational modeling can be profitably used to provide a supporting insight in the design of a bioreactor configuration, according to the following conceptual methodological approach:

> *Task 1):* simulation of the dynamical evolution of the environmental conditions to which cells are subjected, in particular, oxygenation level and shear stress distribution, as a function of the macroscopic control parameters.
>
> *Task 2):* simulation of biomass growth under the action of the above computed biochemical and mechanical stimuli.
>
> *Task 3):* introduction of a feedback mechanism, simulating the effect of the newly formed biomass on the environment (change of geometry, change of nutrient absorption).

In the following, we illustrate in detail how we carry out each item in the above programme, with special care on emphasizing specific contributions of the present research activity compared to existing approaches in the literature. Task 1): in the context of dynamically perfused bioreactors, the implementation of this task requires to couple computational fluid dynamic (CFD) models with diffusion-advection-reaction equations for the nutrient. A starting approach consists of performing a detailed pore-scale CFD simulation to compute the fluid dynamical field over the scaffold walls [34, 31, 41, 6, 3, 24, 42]. These attempts have proven useful in capturing a basic understanding of the conditions which favor the initial development of engineered tissues such as bone [23] and cartilage [34, 35, 33, 36, 27]. Accounting for oxygenation level within the local pore structure is usually carried out by a convection-diffusion-reaction equation where cells are incorporated as sources or sinks of chemical species in the consumption rate in the nutrient mass balance equation [18, 17]. Time evolution of these sources and sinks, representing cell proliferation and migration, is predicted by the use of multicellular algorithms [4, 29]. A significant limitation of this class of models is that the increasing oxygen transfer from the culture medium to the growing cell biomass is included in the mass transport calculation without accounting for

the alteration of the fluid flow due to the growing cell volume (Task 3), so that the above simulation results are valid only for very low cell volume fractions, corresponding to culture conditions at early stages. A further limitation of the pore size-based CFD approach is its validation with respect to experiments. As a matter of fact, microscopic pore and biomass sections are, most often, visually compared to the corresponding results of computational models at the pore size, so that, in order to come up with a quantitative response, a fundamental (and still open) question arises about the statistical significance of the microscopic pore/biomass samples that have been chosen. These limitations are a strong motivation to abandon the analysis at the pure micro-pore level, and replace it with an investigation capable to range from the microscale up to the macroscopic scale, in order to account for the coexistence of multiple temporal and spatial scales, all relevant for the overall behavior of the system. An effective manner to deal with the multiscale behavior of the bioreactor is the so-called Volume Averaging Method (VAM) [44]. The VAM is used in this article as a systematic technique to derive the Stokes-Brinkman equations for perfusion fluid flow and the diffusion-advection-reaction equation for nutrient mass transport, by upscaling to the macroscopic level (over a suitably defined averaging volume) the corresponding microscopic equations. While performing the upscaling procedure, a remarkable bonus provided by the VAM is the identification of "effective" parameters (effective diffusivity and effective hydraulic permeability) which synthetically characterize the system behavior at the macroscopic level by inheriting the properties of the microscale structure. It is in this crucial modeling step that all the available information (geometric, experimental, theoretical) on the sub-scale environment can be profitably used to enhance the accuracy of the upscaled model. Explicit examples of this statement are given later in the discussion of Tasks 2) and 3). Task 2): unlike Task 1), this second task is less consolidated and more open to fundamental questions, since it requires to develop, solve and validate models based on ordinary differential equations (ODE) and/or partial differential equations (PDE) to describe the evolution of the biomass under different stimulating or inhibitory factors. In the present article, we address this issue by the definition of a novel biomass growth model, which is a generalization of the one proposed in [16, 15] through the introduction of the dependence of the biomass growth parameters on the local or mean shear stress. To do this, we carry out a calibration procedure using experimentally measured data previously obtained from one of the Authors [33]. Task 3): this step is a very delicate issue, as it requires, in principle, a detailed representation of the microscale phenomena and their effect on the variation of the porous structure of the scaffold. This problem is dealt with in the present article by the explicit characterization, using the VAM, of the effective nutrient diffusion coefficient and hydraulic permeability as a function of the spatially and time varying volume fraction occupied by the growing biomass [22, 16, 45]. As already remarked in the discussion of Task 2), an important improvement with respect to existing formulations [5] is the direct inclusion of measured data in the

derivation of the model for the effective mass and fluid transport coefficients. In particular, since for the construct we consider [33] the volume fraction occupied by the scaffold porous matrix is significant unlike what assumed in [13, 5], the inclusion of such a term is expected to provide a more accurate prediction of the bioreactor performance, especially in the early stages of culture, where the volume fraction occupied by the growing biomass is small.

2 Material and Methods

Our computational model of the bioreactor structure shown in Fig. 1a encompasses three different phases, a polymeric porous scaffold, a perfusing fluid and a growing biomass, which coexist and evolve in space and time within the cellular construct shown in Fig. 1b. From now on, with the term "biomass" we denote the entire volume of biological matter resulting from cell proliferation and ECM synthesis, and we indicate by ε_s, ε_f and ε_b the scaffold, fluid and biomass volume fractions, respectively. A schematic of the three considered phases is depicted in Fig. 1c, where the averaging volume used for the application of the VAM is represented. Some simplifying assumptions are in order to set up the bioreactor model. We start assuming the volume of the scaffold structure to be time invariant, according to the fact that scaffold degradation is very slow compared to the overall culture time interval, which implies that ε_s is a given constant quantity. Instead, the biomass volume varies with culture time, while consequently the fluid volume is modified in order to satisfy, at each spatial position $\mathbf{x}$ in the construct and at each time t the following constraint

$$\varepsilon_s + \varepsilon_f(\mathbf{x}, t) + \varepsilon_b(\mathbf{x}, t) = 1. \tag{1}$$

To implement Tasks 1)-3), that is, to develop a mathematical model capable to mutually couple biomass growth, oxygen consumption and tissue perfusion, we proceed as follows. First of all, we address Task 2) by proposing a novel biomass growth model that accounts simultaneously for the dependence on oxygen concentration as well as the mechanical stimulus. In order to calibrate the model with respect to this latter quantity we perform a *short term* analysis in which the nutrient concentration and the fluid-dynamic shear stress can be considered constant in time and uniform in space. This allows us to determine the growth model parameters via a fitting procedure. Then, we use the resulting parameters to address Tasks 1) and 3) by a *long term* analysis where the nutrient concentration and perfusion velocity evolve in time and space with tissue growth, consequently modifying the construct properties.

2.1 Biomass growth model

The increase in the biomass volume fraction can be derived starting from the mass conservation principle. This approach can be equivalently applied at different spatial scales. On one side, if the control volume is the entire scaffold,

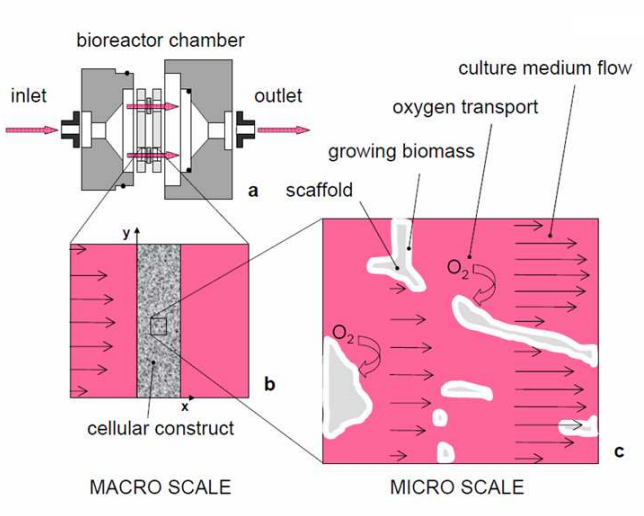

Figure 1: Schematic of the modeled system: bioreactor chamber (a); macroscale representation of the cellular construct (b); details at the microscale level (c).

then the biomass volume fraction that is obtained is a single macroscopic value. On the other side, a point–wise mass balance and a corresponding governing equation can be obtained starting from an infinitesimal control volume centered at point $\mathbf{x}$. At this level, we do not make any difference between these two approaches, although such a difference will become significant as we will distinguish between the short and long term analysis of the engineered tissue growth. Mass conservation allows us to state that biomass growth is governed by the evolution equation

$$\frac{\mathrm{d}\varepsilon_b}{\mathrm{d}t} = (r_g - r_d)\varepsilon_b = r_b\varepsilon_b, \tag{2}$$

where r_d is the death rate accounting for the physiological cell apoptosis, r_g is a growth regulation factor and r_b is the net growth rate. Following [16, 15], in order to model r_g, we use the Monod growth kinetics modified by Contois in [8]

$$r_g(\varepsilon_b, c) = \frac{k_g c}{k_s \rho_b \varepsilon_b + c}, \tag{3}$$

where c is the nutrient (oxygen) concentration, ρ_b is a reference biomass density, k_g is the maximum specific growth rate and k_s is the Contois saturation constant. In [16, 15], the model parameter k_g is adjusted to fit experimental data obtained for different scaffold thicknesses in static culture conditions. As an established model for biomass growth regulation with respect to biomechanical stimuli in dynamical conditions is not yet present in the literature, in our modeling procedure we propose to modify relation (3) in such a way that the parameter k_g is a function of the bio-mechanical stimulus (an averaged or local

shear stress state τ, according to the time span of the analysis) experienced by the cells

$$r_g(\varepsilon_b, c, \tau; p) = \frac{k_g(\tau; p)c}{k_s \rho_b \varepsilon_b + c}, \tag{4}$$

where p denotes a set of unknown parameters to be determined by means of a calibration procedure based on experimental data.

2.2 Short term analysis and model calibration

Assumptions. In order to determine the set of parameters p in Eq.(4), we consider a short term culture time $T = 15$ days. In this working condition, Eq.(2) can be regarded as the mathematical model for the time evolution of the average value of the biomass over the whole construct upon assuming space uniform and time invariant control variables c and τ. These latter hypotheses are legitimate due to the following considerations:

1. the cell volume fraction is small. As a result of that, the oxygen consumption is negligible, which implies that the inlet concentration c_0 (saturation concentration in the fluid) can be used as a representative value for c;

2. the biomass volume fraction is small. As a result of that, the biomass does not yet significantly influence the fluid dynamics shear stresses on the scaffold walls. As a consequence, the median shear stress computed in [37] by CFD models applied to the nude scaffold can be used as a representative value for τ.

Under the above assumptions, the biomass growth model (2)-(4) is uncoupled from nutrient transport and tissue perfusion and can be solved independently.

Model calibration. The experimental set-up for model calibration is the bioreactor system described in [37] and consisting of a bioreactor chamber in which chondrocyte-seeded cellular constructs are fixed on sterile discs, 1 mm in thickness, made of a biodegradable polyestherurethane foam with average porosity 77% [6]. The constructs had their periphery sealed, and were cultured under interstitial perfusion of the culture medium (refer to Fig. 1a for the chamber configuration). Four independent culture chambers were mounted in parallel; culture conditions were identical in each chamber, except for the construct diameter, equal to 2, 3, 4, or 7 mm, respectively. Keeping constant the inlet flow rate for each scaffold yields four different bioreactor configurations, each one being characterized by a given mean inlet velocity v_i, $i = 1, \dots 4$ and by a median shear stress τ_i, this latter quantity being determined by CFD pore-scale simulations [37]. Tab. 1 lists the values of v_i and τ_i, as well as the labels used to identify the four bioreactor configurations. Our calibration procedure is based on the complementary information provided in Figs. 4-a and 4-b of [37], where the DNA and sGAG contents measured at $t = T = 15$ culture days are reported for

each of the four culture conditions A, B, C and D as a function of i, $i = 1, \ldots, 4$. From these data, it is possible to extract the cellular and ECM volume fractions, denoted by $\varepsilon^m_{c,i}$ and $\varepsilon^m_{ECM,i}$, corresponding to the discrete values τ_i and reported as well in Tab. 1. Noting that $\varepsilon^m_{b,i} = \varepsilon^m_{c,i} + \varepsilon^m_{ECM,i}$, we obtain the pairs of data $(\tau_i, \varepsilon^m_{b,i})$, $i = 1, \ldots, 4$, to be used in the parameter fitting for Eq.(2). With this aim, we assume a linear dependence of k_g on the shear stress, *i.e.*

$$k_g = k_{g0}(\alpha + \beta\tau), \tag{5}$$

where k_{g0} is the maximum growth rate in static conditions and α, β are the unknown fitting parameters of our model. Then, letting $p = [\alpha, \beta]$, the vector p_{fit} that best fits in the least square sense the measured values of biomass volume is the solution of the following minimization problem

$$p_{fit} = \arg\min \sum_{i=1}^{4} (\varepsilon_b(T, c, \tau_i; p) - \varepsilon^m_{b,i})^2. \tag{6}$$

Calibration of the cell growth model is carried out by solving Eq.(2) with $k_{g0} = 5.8 \cdot 10^{-6}\text{s}^{-1}$ (corresponding to an average cell division time of 2 days), $k_s = 4.2 \cdot 10^{-3}$ (obtained using the standard Monod kinetics at equilibrium and normalizing the result to the initial value of the biomass fraction as done in [8]) and an apoptosis rate $r_d = 3.85 \cdot 10^{-7}$ s^{-1} (corresponding to an average cell lifetime of 30 days). The initial value of the biomass is set equal to 0.02145 (see Sect. 3 for an extensive discussion of this choice). Using in relation (4) the best fit parameters computed by solving Eq. (6) up to a tolerance of 10^{-5}, the obtained best fit values are $\alpha = 0.8761$ and $\beta = 0.1045$. These results yield in Eq. (5) an amplification factor of the maximum growth rate of about 7 in correspondence of $\tau = \tau_4$. The small reduction of the value of k_g in static conditions ($\tau = 0$) should be ascribed to the fact that no experimental data are available for the fitting procedure in this situation. Fig. 2(top) shows the computed biomass volume fraction as a function of culture time superposed with the experimentally measured quantities at $t = T = 15$ days (denoted by circles), while Fig. 2(bottom) shows the biomass growth rate as a function of culture time as given by Eq. (4).

2.3 Long term analysis: a fully coupled model for biomass growth, tissue perfusion and nutrient transport

Flow of the culture medium. In order to derive a macroscopic description of interstitial fluid flow perfusion throughout the scaffold porous matrix, we introduce the following assumptions:

1. low perfusion regimes. This allows us to neglect inertial terms in the momentum balance equation;

2. the scaffold and biomass are rigid and impermeable to the fluid. This allows us to treat the fluid problem as a homogenized biphasic system (fluid and solid phases).

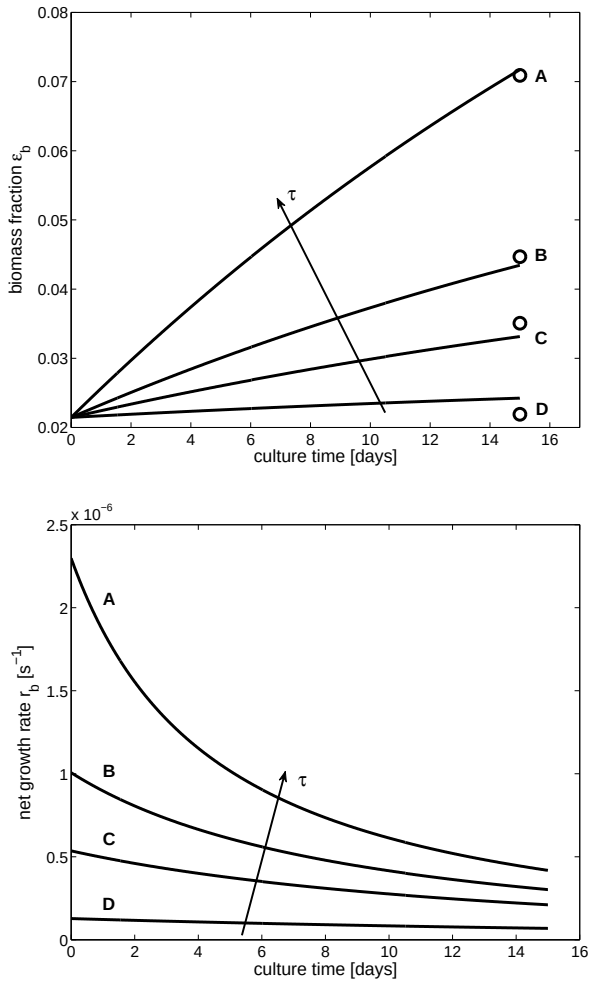

Figure 2: Biomass volume fraction ε_b (top) and cell growth rate r_b (bottom) as a function of culture time. The plots are obtained from the short–time model by solving Eq.(2), with the coefficients given in relation (4) and using the best fit parameters solution of Eq.(6).

Table 1: Scaffold configurations for model calibration (from [37]).

Scaffold diameter [cm]	Label	Index i	Inlet velocity v_i [cm/s]	Median shear stress τ_i [mPa]	Cell volume fraction	ECM volume fraction
0.2	A	1	0.884	56	0.0343	0.0366
0.3	B	2	0.393	25	0.0216	0.0231
0.4	C	3	0.221	14	0.0164	0.0187
0.7	D	4	0.072	4.6	0.0094	0.0125

Applying the VAM over the averaging volume of Fig. 1c, yields the following macroscopic Stokes equation system with Brinkman correction [22, 46]

$$\begin{aligned} &\nabla \cdot \mathbf{v} = 0, \\ &\nabla p = -\mu \varepsilon_f K^{-1}(\varepsilon_f)\mathbf{v} + \mu \triangle \mathbf{v}, \end{aligned} \tag{7}$$

where μ is the dynamic viscosity of the culture medium, $\mathbf{v}$ is the Darcy velocity, p is the fluid pressure and K is the effective hydraulic permeability. An established closure relation expressing K as a function of the space and time dependent fluid volume fraction ε_f (related to the solid volume fraction by Eq. (1)) is provided by the Carman-Kozeny equation [2, 22, 46]

$$K(\varepsilon_f) = K_p \frac{\varepsilon_f^3}{(1-\varepsilon_f)^2}, \tag{8}$$

where the Kozeny constant K_p is a reference permeability to be later specified.

To achieve a full coupling with biomass growth, the interstitial perfusion model must be complemented with a precise definition of the expression of shear stress to be used in the context of VAM averaged equations. In the context of low perfusion regimes, an acceptable model is an adaptation of the Darcy-Carman-Kozeny formula proposed in [43] to the case of a variable permeability

$$\tau(\varepsilon_b, |\mathbf{v}|) = \frac{\mu |\mathbf{v}|}{\sqrt{K(\varepsilon_f)}} = \frac{\mu |\mathbf{v}|}{\sqrt{K(1-\varepsilon_s-\varepsilon_b)}}. \tag{9}$$

The above formula connects in an almost linear fashion the variation of the average shear stresses on the porous matrix walls to the average filtration velocity, as expected in these flow regimes. Moreover, the formula establishes a dependence

of the stress on the actual biomass fraction. In order to characterize the Kozeny permeability K_p required to compute the effective hydraulic permeability given by Eq. (8), we use again a least square fitting between the values predicted by Eq. (9) by setting $\varepsilon_b = 0$ and $|\mathbf{v}|_i = v_i$, where v_i, $i = 1, ..., 4$ are the inlet velocities listed in Tab. 1, and the median (pore-scale) shear stress computed in [37] and reported in Tab. 1. More precisely, we aim to find

$$K_{p,fit} = \arg\,\min \sum_{i=1}^{4} \left(\tau(0, |\mathbf{v}|_i) - \tau_i\right)^2.$$

The best fit value is $K_{p,fit} = 1.97 \cdot 10^{-7}$ cm^2, which produces an extremely accurate fitting, the corresponding residual being of the order of 10^{-10}. The functions $\tau(\varepsilon_b, |\mathbf{v}|_i)$ obtained from relation (9) using the optimal value of $K_{p,fit}$ are plotted in Fig. 3 in correspondence of $|\mathbf{v}|_i = v_i$, $i = 1, ..., 4$, showing that the shear stress is an increasing function of the biomass fraction, consistently with the fact that hydraulic resistance increases with cell proliferation. This analysis is particularly interesting in our case, because it provides an indication of the range of construct porosities where the present model can be considered to be reliable according to experimental validation. Indeed, it suggests that for long term cultures, where the biomass volume fraction is expected to grow significantly, only experiments with moderate inlet velocity, i.e. values C, D of Tab. 1, would correspond to shear stresses in the range where the present biomass growth model has been validated.

Oxygen mass transport. Applying again the VAM over the averaging volume of Fig. 1c, and neglecting accumulation terms, yields the following mass conservation law in advective-diffusive-reactive form for the volume averaged oxygen concentration, c, in the homogenized phase

$$\nabla \cdot (-D\nabla c + \mathbf{v}c) + R(c) = 0, \tag{10}$$

where $c = \varepsilon_s c_s + \varepsilon_f c_f + \varepsilon_b c_b$, and c_f, c_b are the volume averaged oxygen concentrations in the fluid and biomass phases, respectively, c_s is the negligible oxygen concentration inside the scaffold, $\mathbf{v}$ is the fluid velocity predicted by (7), and R is the biomass oxygen volumetric consumption rate, which is assumed to be a function of the local oxygen concentration according to the Michaelis-Menten kinetics

$$R(c) = \frac{R_m c}{K_m + c}\varepsilon_b, \tag{11}$$

R_m and K_m being the maximal consumption rate and the half saturation constant, respectively. The effective diffusivity D in Eq. (10) can be characterized as in [45], resorting to an approximate solution of the so called closure problem. Applying such an approach in a multiphase system like the one at hand (where we have three phases: fluid, biomass and solid scaffold) is a very challenging

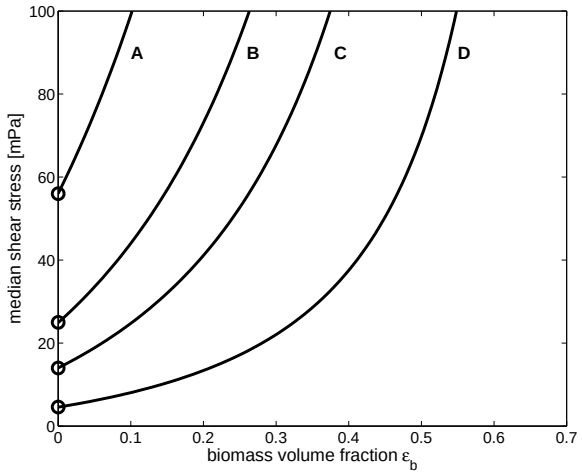

Figure 3: Plot of the increase of shear stresses induced by biomass volume fraction growth. Each curve corresponds to a different value of the average velocity, equal to the inlet velocities A, B, C, D of Tab. 1, from top to bottom. The reference median shear stress values of Tab. 1 are highlighted with circle markers on the y axis.

problem. However, for the specific problem at hand, we point out some realistic assumptions that allow us to simplify this process:

1. the scaffold matrix is impermeable to oxygen. This is equivalent to assuming that the oxygen diffusivity into the scaffold is negligible. This also allows us to conclude that the oxygen concentration into the scaffold is vanishing.

2. the diffusivity of oxygen in the fluid phase is almost equivalent to the one in the biomass [28]. We notice that this property would not be valid for molecules considerably larger than oxygen, such as glucose.

Owing to these assumptions, we can consider a biphasic system made of a "fluid-equivalent phase" (culture medium + biomass) and a solid phase (scaffold), i.e. we have $c = \varepsilon_f c_f + \varepsilon_b c_b$ since $c_s = 0$ and define $\varepsilon_{fb} = \varepsilon_f + \varepsilon_b$ and $c_{fb} = \varepsilon_f c_f + \varepsilon_b c_b$, c_{fb} being the average concentration of the "fluid-equivalent phase". We notice that $c = c_{fb}$ in this particular case.

Then, we use Maxwell's model [26, 45] to find a closure relation for the diffusive flux into a biphasic system characterized by the scaffold and by a "fluid-equivalent phase". More precisely, we define the diffusive flux as

$$\mathbf{j} = -D\nabla c = -D_{fb}\nabla c_{fb} \tag{12}$$

where $D = D_{fb}$ is the effective diffusivity to be suitably approximated. We focus on the equivalent problem of determining D_{fb}, that is the effective diffusivity

relative to the "fluid-equivalent phase" average concentration. Since we assume that the diffusivity of oxygen in the fluid is almost equivalent to the one in the biomass we denote with $D'_f = D'_b = D'_{fb}$ the diffusivity of oxygen into a medium composed by either pure fluid or pure biomass or any mixture of these components. Maxwell model states that

$$\frac{D_{fb}}{D'_{fb}} = M\big(\varepsilon_{fb}, \kappa_{fb}\big), \quad \kappa_{fb} = k_{eq}\frac{D'_s}{D'_{fb}}$$

where $M(\varepsilon, \kappa)$ denotes Maxwell's formula [26]. and k_{eq} is a suitable equilibrium constant, see [45]. However, the value of k_{eq} is irrelevant for us, because we assume that oxygen does not diffuse into the scaffold, hence $D'_s = 0$ and $\kappa_{fb} = 0$ for any possible finite value of k_{eq}. In the case where the scaffold resembles to an array of disjoint spheres, we use

$$M(\varepsilon) = \frac{3\kappa - 2\varepsilon(\kappa - 1)}{3 + \varepsilon(\kappa - 1)},$$

while in the case it resembles to an array of cylinders, we use

$$M(\varepsilon) = \frac{2\kappa - \varepsilon(\kappa - 1)}{2 + \varepsilon(\kappa - 1)}.$$

We believe that in our case the former formula is more appropriate. Combining the previous expressions, we finally obtain

$$\frac{D}{D'_f} = \frac{2(1 - \varepsilon_s)}{2 + \varepsilon_s}$$

where D'_f is the oxygen diffusivity in the pure fluid phase, which can be easily determined by measurements. We also notice that, in this specific case, the effective diffusivity coefficient, D, only depends on the scaffold volume fraction ε_s. This is a direct consequence of the assumption that the nutrient diffuses equivalently in the fluid and in the biomass.

Solution algorithm and numerical approximation. Let N be the number of time subdivisions of the culture time interval $[0, T]$, $\Delta t = T/N$ the time step and $t^k = k\Delta t$ the k-th time level, $k = 0, \ldots, N$. Then, the solution of the time–dependent nonlinear coupled system describing engineered tissue growth under interstitial nutrient flow and constituted by the ODE (2) and by the PDEs (7) and (10) is reduced to the solution of a sequence of decoupled linearized sub-problems according to the following block Gauss–Seidel iteration:
Given $\varepsilon_b^n = \varepsilon_b(t^n)$, $\mathbf{v}^n = \mathbf{v}(t^n)$ and $c^n = c(t^n)$, for all $n = 0, \ldots, N - 1$:

Step 1: solve the Stokes-Brinkman problem

$$\nabla \cdot \mathbf{v}^{n+1} = 0,$$
$$\nabla p^{n+1} = -\mu \varepsilon_f^n K^{-1}(\varepsilon_f^n)\mathbf{v}^{n+1} + \mu \triangle \mathbf{v}^{n+1},$$

and then set $\mathbf{v}(t^{n+1}) = \mathbf{v}^{n+1}$ and $p(t^{n+1}) = p^{n+1}$.

Step 2: solve the nutrient balance equation

$$\nabla \cdot (-D\nabla c^{n+1} + \mathbf{v}^{n+1} c^{n+1}) + R(c^n) = 0,$$

and then set $c(t^{n+1}) = c^{n+1}$.

Step 3: compute the Darcy stress

$$\tau^{n+1} = \frac{\mu |\mathbf{v}^{n+1}|}{\sqrt{K(1 - \varepsilon_s - \varepsilon_b^n)}}$$

and then set $\tau(t^{n+1}) = \tau^{n+1}$.

Step 4: solve the biomass growth equation using a one-step explicit time–marching method

$$\frac{\varepsilon_b^{n+1} - \varepsilon_b^n}{\Delta t} = \Phi_b(\varepsilon_b^n, c^{n+1}, \tau^{n+1}; \Delta t)$$

Φ_b being a suitable increment function, and then set $\varepsilon_b(t^{n+1}) = \varepsilon_b^{n+1}$.

The temporal stability of the above solution algorithm is determined by the appropriate choice of Δt. To this purpose, we first need to study the stability properties of the biomass growth model (2). For this analysis, we assume c and τ to be parameters allowed to vary in the admissible space $\mathcal{P} = (0, c_0] \times [\tau_4, \tau_1]$ and set $f(\varepsilon_b) := r_b \varepsilon_b$. The equation $f(\varepsilon_b) = 0$ has two roots, $\varepsilon_{b,1} = 0$ and

$$\varepsilon_{b,2}(c, \tau) = \frac{c(k_g(\tau) - r_d)}{r_d \rho_b k_s}.$$

It is easy to verify that, since $k_g(\tau) - r_d > 0$ for all $\tau \in [\tau_1, \tau_4]$, $\varepsilon_{b,2} > 0$. To investigate the mathematical nature of the two equilibrium points, we consider the linearized version of the growth model (2) [1]

$$\frac{d\varepsilon_b}{dt} = \lambda(\varepsilon_b; c, \tau)\varepsilon_b + g$$

where g is an inhomogeneous term that has no influence on the stability of the problem, and

$$\lambda(\varepsilon_b; c, \tau) := \frac{\partial f}{\partial \varepsilon_b} = \frac{k_g(\tau) c^2}{(k_s \rho_b \varepsilon_b + c)^2} - r_d.$$

Replacing into the above formula the expressions of the equilibrium points yields $\lambda(\varepsilon_{b,1}; c, \tau) = k_g(\tau) - r_d > 0$ for all τ and $\lambda(\varepsilon_{b,2}; c, \tau) = r_d(r_d - k_g(\tau))/k_g(\tau) < 0$, from which we conclude that $\varepsilon_{b,1}$ is an unstable equilibrium point while $\varepsilon_{b,2}$ is an asymptotically stable equilibrium point. We can now turn to the analysis of the scheme in Step 4, which is the discrete counterpart of problem (2), and we investigate its absolute stability in the sense of Dahlquist [9]. For ease of presentation, we consider the simplest case of the Forward Euler (FE) method, corresponding to $\Phi_b = r_b(\varepsilon_b^n)\varepsilon_b^n$. The study of the sign of λ reveals that $\lambda < 0$ provided that $\varepsilon_b > \varepsilon_{b,lim} = c((k_g(\tau)/r_d)^{1/2} - 1)/(k_s \rho_b)$, condition that is largely satisfied by the initial value ε_b^0 for every choice of $(c, \tau) \in \mathcal{P}$. In particular, we need to characterize the maximum absolute value of λ. This occurs at $\varepsilon_b = \varepsilon_{b,2}$, in correspondence of $\tau = \tau_1$ and irrespective of the value of the nutrient concentration c. Moreover, setting $\mathcal{I}_\varepsilon = [\varepsilon_{b,lim}, \varepsilon_{b,2}]$, we have

$$\max_{\substack{\varepsilon_b \in \mathcal{I}_\varepsilon; \\ (c,\tau) \in \mathcal{P}}} |\lambda(\varepsilon_b; c, \tau)| = r_d \left(1 - \frac{r_d}{k_g(\tau_1)}\right) < r_d := \lambda_{max},$$

so that we can conclude that the FE method in Step 4 is absolutely stable, provided that

$$\Delta t < \frac{2}{\lambda_{max}} = 60 \text{ days},$$

which by far exceeds the actual time step used due to accuracy requirements in the simulations. We notice that a similar analysis applies if a higher-order one-step explicit method is used in Step 4, for instance, a 4th–order Runge–Kutta method.

The spatial discretization of each PDE subproblem in the solution algorithm Steps 1-4 is carried out using the Galerkin Finite Element Method (see, e.g., [32]). In particular, the stable Taylor-Hood pair is used for the approximation of fluid velocity and pressure in Step 1, while piecewise linear elements are used for the approximation of the nutrient concentration in Step 2.

3 Results

The numerical simulations have been carried out by coding the algorithm Steps 1-4 within the Matlab software environment. The geometry of the computational domain is shown in Fig. 4, along with the boundary conditions. In Fig. 4, W is the scaffold thickness, taken equal to 1mm as in the experimental devices described in Sect. 2.2, while H is the scaffold diameter, chosen as in Tab. 1 for the different configurations. Moreover, $\mathbf{n}$ is the outward unit normal vector, $\mathbf{j}$ is

the diffusive flux for the concentration field defined in (12) and $\mathbf{T} = 2\mu\boldsymbol{\varepsilon}(\mathbf{v}) - p\mathrm{Id}$ is the stress tensor, where $\boldsymbol{\varepsilon}(\mathbf{v})$ and Id denote the rate–of–strain tensor of the velocity field and the identity matrix, respectively. The inlet velocity field is a plug flow of modulus v_{in} (see Tab. 1). Numerical simulations carried out adding prior to the scaffold inlet section ($x = 0$) a sufficiently long tract where a clear fluid flows, demonstrate that this is a reasonable choice for the entrance fluid velocity profile. The initial biomass volume fraction is computed from the prescribed total number N_{cells} of seeded cells, supposing that at $t = 0$ the biomass is constituted only by cells. Cells can be seeded uniformly in the scaffold or be unevenly distributed. In the first case, denoting by $V_{cell} = \frac{4}{3}\pi(H_{cell}/2)^3$ the volume of the single cell, H_{cell} being the cell diameter, and by $V_{scaff} = \pi(H/2)^2 W$ the scaffold volume, the density of seeded cells can be straightforwardly computed as $\varepsilon_b^0 = N_{cells}\frac{V_{cell}}{V_{scaff}} = 0.02145$. The second case is discussed in detail later in the section. In the numerical simulations, only scaffold configurations C and D are considered, in accordance with the previously drawn conclusions that the calibration of the full model is valid only for moderate median shear stresses. The values of the model parameters are listed in Tab. 2.

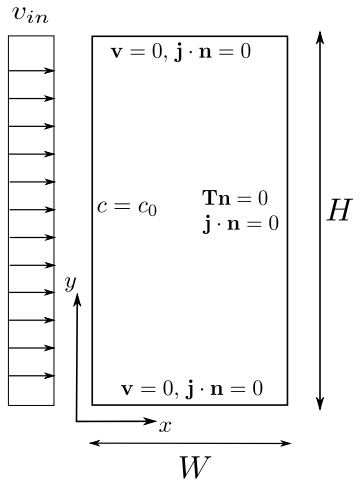

Figure 4: Geometry of the domain and boundary conditions for the numerical simulations of the PDE/ODE model.

The first set of results refers to uniform seeding conditions. Fig. 6 illustrates the comparison between predictions of the average biomass volume fraction (defined as the mean integral value of $\varepsilon_b(\mathbf{x}, t)$ over the scaffold area at each time t) obtained by running the sole ODE model (2) (dashed lines) and the full PDE/ODE model described in Steps 1-4 (solid lines) up to a final culture time of $T = 90$ days. The discrepancy between the two models is related to the effect of the shear stresses, which are higher in the fully–coupled model predictions with respect to the fixed value considered in the simple ODE model, because

Table 2: Numerical values of the parameters used in the simulations.

Parameter	Dimension	Definition	Value	Ref.
c_0	[g/cm^3]	culture medium inlet O2 concentration	$6.4{\cdot}10^{-6}$	[28]
D_f	[cm^2/s]	O_2 diffusivity in H_2O and biomass at 37°C	$2.1{\cdot}10^{-5}$	[28]
N_{cells}	[ ]	number of seeded cells	$8 \cdot 10^4$	[37]
H_{cell}	[mm]	diameter of the cell	$8{\cdot}10^{-3}$	[37]
ε_s	[ ]	scaffold volume fraction	0.23	[37]
k_d	[1/s]	cell death rate	$1/(30 \cdot 24 \cdot 3600)$	[16]
k_{g0}	[1/s]	maximum specific cell growth rate	$1/(2 \cdot 24 \cdot 3600)$	[28]
k_s	[ ]	Contois cell saturation constant	$4.2 \cdot 10^{-3}$	
μ	[g/cm/s]	culture medium dynamic viscosity at 37°C	$8.26{\cdot}10^{-3}$	[34]
ρ_b	[g/cm^3]	reference biomass density	1	
R_m	[1/s]	O_2 maximal consumption rate	$3.9{\cdot}10^{-8}$	[7]
K_m	[g/cm^3]	O_2 half saturation constant	$3.2{\cdot}10^{-6}$	[28]

of the variation of permeability caused by the increasing biomass. Moreover, as biomass production and increase of stress are mutually coupled in a positive feedback loop, discrepancies are more significant in scaffold C, where the velocity field is higher. Fig. 7 shows the median Darcy stresses obtained by the PDE/ODE model as a function of culture time. Fig. 8 shows for scaffold C how the increased biomass fraction affects the shear stress distribution pattern. At advanced cell growth stages, as expected, higher shear values are recorded. Moreover, a narrower distribution of the values is observed, in accordance with the results of [24]. Figs. 9 and 10 refer again to the scaffold configuration C, and show the snapshots of the spatial distribution, at various culture times, of the normalized oxygen concentration field and the biomass volume fraction (sampled at $y = H/2$).

The second set of results aims to investigate the effects of a non–uniform initial seeding of cells in the scaffold. To this purpose, we keep constant the total number of cells as indicated in Tab. 2, while we allow the density of seeding to be a function of the spatial position inside the scaffold domain, so that also the initial biomass volume fraction is a function of the spatial position. In particular, we suppose to have a certain seeding density ρ_1 in a cylindrical central region of diameter H_i of the 3D scaffold and a different seeding density ρ_2 in the remaining surrounding toroidal region (see Fig. 5).

The two densities are related by the convex combination

$$\frac{\rho_1}{\rho_{seed}}\xi^2 + \frac{\rho_2}{\rho_{seed}}(1-\xi^2) = 1,$$

where $\xi = H_i/H$ and $\rho_{seed} = N_{cells}/V_{scaff}$ is the cell density in the uniform seeding case. We set $\xi = 0.5$ and consider the scaffold configuration C. Then we carry out a first set of simulations choosing $\rho_1 = 2\rho_{seed}$, corresponding to $\rho_2 = \frac{2}{3}\rho_{seed}$, so that the cell seeding density is higher in the central region, and a second set of simulations in the opposite situation with $\rho_1 = 0.5\rho_{seed}$,

corresponding to $\rho_2 = \frac{5}{4}\rho_{seed}$. In Fig. 11, we represent the 3D surf plot of the biomass volume fraction at $t = 7, 30, 90$ days of culture, from bottom to top, respectively, for the case $\rho_1 = 2\rho_{seed}$, while in Fig. 12, we represent the results in the case $\rho_1 = 0.5\rho_{seed}$. In both conditions, after an initial transient, the distribution of the biomass volume fraction tends to become homogeneous over the domain, because of the greater availability of nutrient in the scaffold regions less densely seeded, which in turn promotes biomass growth.

4 Discussion and conclusions

The aim of this work was to set up a multiphysics/multiscale computational model for the simulation of the process of biomass growth in an engineered cartilaginous construct, cultured under interstitial perfusion in a bioreactor. The model comprises three phases: cells and ECM (treated as a single phase, biomass), the culture medium, and the time–invariant scaffold porous structure, and it provides a self–consistent coupling among the fluid-dynamical environment, the nutrient delivery and consumption and the biomass growth. Compared to previous pore–scale CFD simulations, this approach allows to study long-term interstitial perfusion in scaffolds with high cell volume fractions, at affordable computational costs, and to perform simulations for any scaffold pore geometry, regular (for example the idealized scaffold pore structures considered in [3, 24]) or irregular (for example the ones obtained from the μCT images of [38]).

Concerning the critical issue of the description of the temporal and spatial evolution of the developing biomass, our approach is based on the fundamental experimental observation that in perfused bioreactors biomass growth is influenced primarily by two factors, oxygen tension and fluid dynamical shears [39]. While the role of oxygen delivery to cells has been extensively investigated in several computational studies (see for example, [16, 15, 12]), considerably less attention has been paid to account for the effect of mechanical stimuli in the prediction of biomass growth. Therefore, in this article, we have focused our analysis on the extension of the Monod growth model proposed in [16, 15], in such a way that the coupling of cell behavior and mechanical environment is captured through the introduction of a stress–dependent relation for the specific growth rate. The parameters entering such relation have been calibrated on the experimental data of [33] using a simplified reduced model for which the nutrient and stress distributions are assumed to be constant in time and uniform in space, consistently with the environmental conditions of the early culture times of [33]. The simplified growth model is also used as a paradigm for investigating the stability of the functional iteration employed to successively solve the fully–coupled ODE/PDE problem.

In the derivation of the fully–coupled model, the VAM is systematically employed to obtain macroscopic equations which keep into account microscopic

scale contributions by an appropriate definition of effective parameters, such as hydraulic permeability and nutrient diffusivity. Concerning with the permeability, similarly to what done for the biomass growth model, a calibration procedure is carried out to determine its reference value, in such a way that the range of values attained by the correspondingly computed Darcy stresses are compatible with the pore–scale analysis of [33]. This approach allows to overcome a critical issue arising in the comparison between shear stress predictions of microscale vs. macroscale approaches (see [6, 5]). As for the effective oxygen diffusivity, a simplified two–phase model comprising a solid phase (scaffold) and a "fluid–equivalent" phase (biomass and perfusion medium) has been considered, so that the theory of [45] can be applied to the problem at hand to yield a closed expression for the nutrient diffusion coefficient.

An extensive numerical validation of the above described computational model has been carried out. Our results can be directly compared to those obtained in [5], even if in this reference the effect of the shear stress in the growth model as well as of the presence of the scaffold volume fraction in the calculations of the permeability were not considered. The computed increase in biomass volume fraction with culture time is in good qualitative agreement with published data from perfusion experiments [10, 14, 25]. Only qualitative agreement may be expected in this regard, because the flow rates, scaffold materials, cell densities and culture medium compositions differ among the various studies. Also, most bioreactor studies are based on the comparison, at the end of cultivation, of constructs subjected to perfused versus non perfused conditions.

Future developments will include 2D axisymmetric and 3D implementations of the model, a more thorough investigation of the biomass growth model, featuring independent balance equations for the cellular and the extracellular fractions, and the development of new experimental protocols to be interfaced to the numerical simulations. Transport of solutes other than oxygen can be easily added due to the modular structure of the simulation tool.

References

[1] Arnold, V.: Ordinary Differential Equations. The MIT Press, Cambridge, Massachusetts (1973)

[2] Bear, J.: Dynamics of Fluids in Porous Materials. American Elsevier, New York (1972)

[3] Boschetti, F., Raimondi, M.T., Migliavacca, F., Dubini, G.: Prediction of the micro-fluid dynamic environment imposed to three-dimensional engineered cell systems in bioreactors. J. Biomech. **39**(3), 418–425 (2006)

[4] Cheng, G., Youssef, B., Markenscoff, P., Zygourakis, K.: Cell population dynamics modulate the rates of tissue growth processes. Biophys Jour **90**(3), 713–724 (2007)

[5] Chung, C., Chen, C., Chen, C., Tseng, C.: Enhancement of cell growth in tissue-engineering constructs under direct perfusion: Modeling and simulation. Biotechnology and Bioengineering **97**(6), 1603–1616 (2007)

[6] Cioffi, M., Boschetti, F., Raimondi, M.T., Dubini, G.: Modeling evaluation of the fluid-dynamic microenvironment in tissue-engineered constructs: a micro-CT based model. Biotechnol. Bioeng. **93**(3), 500–510 (2006)

[7] Cioffi, M., Kueffer, J., Stroebel, S., Dubini, G., Martin, I., Wendt, D.: Computational evaluation of oxygen and shear stress distributions in 3d perfusion culture systems: Macro-scale and micro-structured models. Journal of Biomechanics **41**(14), 2918 – 2925 (2008)

[8] Contois, D.E.: Kinetics of bacterial growth: Relationship between population density and specific growth rate of continuous cultures. J. Gen. Microbiol. **21**, 40–50 (1959)

[9] Dahlquist, G., Bjorck, A.: Numerical Methods. Dover, New York (2003)

[10] Davisson, T., Sah, R., Ratcliffe, A.: Perfusion increases cell content and matrix synthesis in chondrocyte three-dimensional cultures. Tissue Engineering **8**(5), 807–816 (2002)

[11] Dunkelman, N., Zimber, M., Lebaron, R., Pavelec, R., Kwan, M., Purchio, A.: Cartilage production by rabbit articular chondrocytes on polyglycolic acid scaffolds in a closed bioreactor system. Biotech. Bioeng. **46**, 299–305 (1995)

[12] Freed, L., Vunjak-Novakovic, G.: Tissue engineering bioreactors. In: R.P. Lanza, R. Langer, J. Vacanti (eds.) Principles of tissue engineering. Academic Press, San Diego (2000)

[13] Freed, L., Vunjak-Novakovic, G., Marquis, J., Langer, R.: Kinetics of chondrocyte growth in cell-polymer implants. Biotechnology and Bioengineering **43**(7), 597–604 (1994)

[14] Freyria, A.M., Yang, Y., Chajra, H., Rousseau, C., Ronzire, M.C., Herbage, D., Haj, A.E.: Optimization of dynamic culture conditions: Effects on biosynthetic activities of chondrocytes grown in collagen sponges. Tissue Engineering **11**(5-6), 674–684 (2005)

[15] Galban, C.J., Locke, B.R.: Analysis of cell growth kinetics and substrate diffusion in a polymer scaffold. Biotechnology and Bioengineering **65**(2), 121–132 (1999)

[16] Galban, C.J., Locke, B.R.: Effects of spatial variation of cells and nutrient product concentrations coupled with product inhibition on cell growth in a polymer scaffold. Biotechnology and Bioengineering **64**(6), 633–643 (1999)

[17] Galbusera, F., Cioffi, M., Raimondi, M.T.: An in silico bioreactor for simulating laboratory experiments in tissue engineering. Biomedical Microdevices **10**(4), 547–554 (2008)

[18] Galbusera, F., Cioffi, M., Raimondi, M.T., Pietrabissa, R.: Computational modelling of combined cell population dynamics and oxygen transport in engineered tissue subject to interstitial perfusion. Computer Methods in Biomechanics and Biomedical Engineering **10**(4), 279–287 (2007)

[19] Grodzinsky, A., Levenston, M., Jin, M., Frank, E.: Cartilage tissue remodeling in response to mechanical forces. Annual Review of Biomedical Engineering **2**(1), 691–713 (2000)

[20] Guilak, F., Hung, C.: Basic orthopaedic biomechanics and mechano-biology, chap. Physical regulation of cartilage metabolism, pp. 259–300. Lippincott Williams and Wilkins (2005)

[21] Haj, A.J.E., Wood, M.A., Thomas, P., Yang, Y.: Controlling cell biomechanics in orthopaedic tissue engineering and repair. Pathologie Biologie **53**(10), 581 – 589 (2005)

[22] Hsu, C., Cheng, P.: Thermal dispersion in a porous medium. Int. J. Heat Mass Transfer **33**(8), 1587–1597 (1990)

[23] Leclerc, E., David, B., Griscom, L., Lepioufle, B., Fujii, T., Layrolle, P., Legallaisa, C.: Study of osteoblastic cells in a microfluidic environment. Biomaterials **27**(4), 586 – 595 (2006)

[24] Lesman, A., Blinder, Y., Levenberg, S.: Modeling of flow-induced shear stress applied on 3D cellular scaffolds: implications for vascular tissue engineering. Biotechnology and Bioengineering **105**(3), 645–654 (2010)

[25] Mahmoudifar, N., Doran, P.: Tissue engineering of human cartilage and osteochondral composites using recirculation bioreactors. Biomaterials **26**, 7012–7024 (2005)

[26] Maxwell, J.: Treatise on electricity and magnetism, vol. I. Clarendon Press, Oxford (1881). Reprinted by Dover, New York, 1954

[27] Moretti, M., Freed, L., Padera, R., Laganà, K., Boschetti, F., Raimondi, M.: An integrated experimentalcomputational approach for the study of engineered cartilage constructs subjected to combined regimens of hydrostatic pressure and interstitial perfusion. Bio-Medical Materials and Engineering **22**(18(4)), 273–278 (2008)

[28] Palsson, B., Bhatia, S.: Tissue engineering, chap. Scaling up for ex vivo cultivation, pp. 223–243. Pearson Education (2004)

[29] Palsson, E.: A three-dimensional model of cell movement in multicellular systems. Future Gener. Comput. Syst. **17**(7), 835–852 (2001). DOI http://dx.doi.org/10.1016/S0167-739X(00)00062-5

[30] Pazzano, D., Mercier, K., Moran, J., Fong, S., DiBiasio, D., Rulfs, J., Kohles, S., Bonassar, L.: Comparison of chondrogensis in static and perfused bioreactor culture. Biotechnology Progress **16(5)**, 893–896 (2000)

[31] Porter, B., Zauel, R., Stockman, H., Guldberg, R., Fyhrie, D.: 3-d computational modeling of media flow through scaffolds in a perfusion bioreactor. Journal of Biomechanics **38**(3), 543 – 549 (2005)

[32] Quarteroni, A., Valli, A.: Numerical Approximation of Partial Differential Equations (2nd Ed.). Springer-Verlag, New York (1997)

[33] Raimondi, M.: Engineered tissue as a model to study cell and tissue function from a biophysical perspective. Current Drug Discovery Technologies **3**(4), 245–68 (2006)

[34] Raimondi, M., Boschetti, F., Falcone, L., Fiore, G., Remuzzi, A., Marinoni, E., Marazzi, M., Pietrabissa, R.: Mechanobiology of engineered cartilage cultured under a quantified fluid-dynamic environment. In: Biomechanics and modeling in mechanobiology, vol. 1, pp. 69–82. Springer-Verlag, Berlin, Germany (2002)

[35] Raimondi, M., Boschetti, F., Falcone, L., Migliavacca, F., Remuzzi, A., Dubini, G.: The effect of media perfusion on three-dimensional cultures of human chondrocytes: integration of experimental and computational approaches. Biorheology **41**(3-4), 401–10 (2004)

[36] Raimondi, M., Candiani, G., Cabras, M., Cioffi, M., Laganà, K., Moretti, M., Pietrabissa, R.: Engineered cartilage constructs subject to very low regimens of interstitial perfusion. Biorheology **45**(3-4), 471–9 (2008)

[37] Raimondi, M., Moretti, M., Cioffi, M., Giordano, C., Boschetti, F., Laganà, K., Pietrabissa, R.: The effect of hydrodynamic shear on 3d engineered chondrocyte systems subject to direct perfusion. Biorheology **43**(3-4), 215–22 (2006)

[38] Raimondi, M.T., Boschetti, F., Migliavacca, F., Cioffi, M., Dubini, G.: Micro fluid dynamics in three-dimensional engineered cell systems in bioreactors. In: N. Ashammakhi, R.L. Reis (eds.) Topics in Tissue Engineering, vol. 2, chap. 9 (2005)

[39] Schulz, R., Bader, A.: Cartilage tissue engineering and bioreactor systems for the cultivation and stimulation of chondrocytes. Eur. Biophys. J. **36**, 539–568 (2007)

[40] Silver, F.: Mechanosensing and Mechanochemical Transduction in Extracellular Matrix, chap. Mechanochemical Sensing and Transduction, pp. 211–261. Springer US (2006)

[41] Singh, H., Teoh, S., Low, H., Hutmacher, D.: Flow modelling within a scaffold under the influence of uni-axial and bi-axial bioreactor rotation. Journal of Biotechnology **119**(2), 181 – 196 (2005)

[42] Vossenberg, P., Higuera, G., van Straten, G., van Blitterswijk, C., van Boxtel, A.: Darcian permeability constant as indicator for shear stresses in regular scaffold systems for tissue engineering. Biomechanics and Modeling in Mechanobiology **8**(6), 499–507 (2009)

[43] Wang, S., Tarbell, J.: Effect of fluid flow on smooth muscle cells in a 3-dimensional collagen gel model. Arteriosclerosis, thrombosis, and vascular biology **20**(10), 2220–2225 (2000)

[44] Whitaker, S.: The method of volume averaging. Theory and application of transport in porous media. Kluwer Academic Publishers (1999)

[45] Wood, B.D., Quintard, M., Whitaker, S.: Calculation of effective diffusivities for biofilms and tissues. Biotech. and Bioeng. **77**(5), 495–514 (2002)

[46] Wood, B.D., Whitaker, S.: Diffusion and reaction in biofilms. Chem. Eng. Sci. **53**, 397–425 (1998)

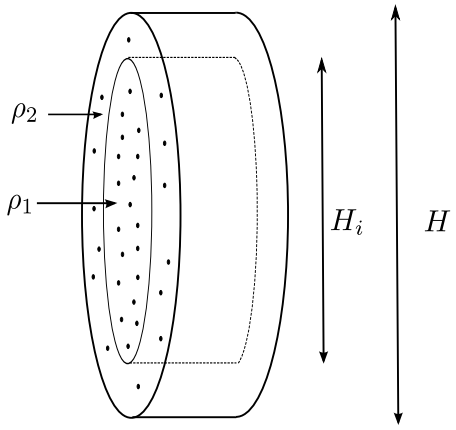

Figure 5: Geometry and notation for the non–uniform seeding case study.

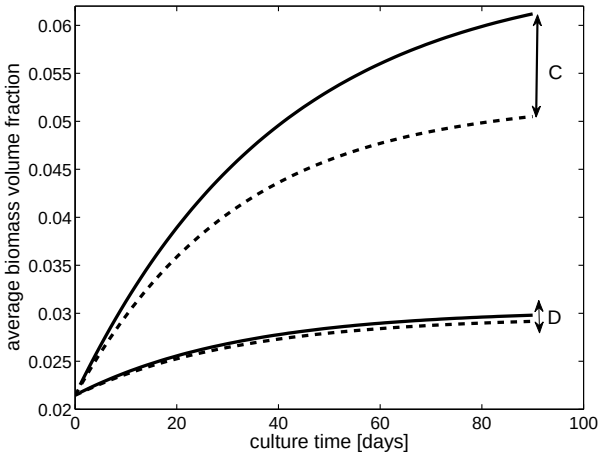

Figure 6: Comparison between average biomass fraction predictions as a function of culture time obtained using different computational models. Dashed lines refer to the ODE model (2), while solid lines refer to the PDE/ODE model described in Steps 1-4.

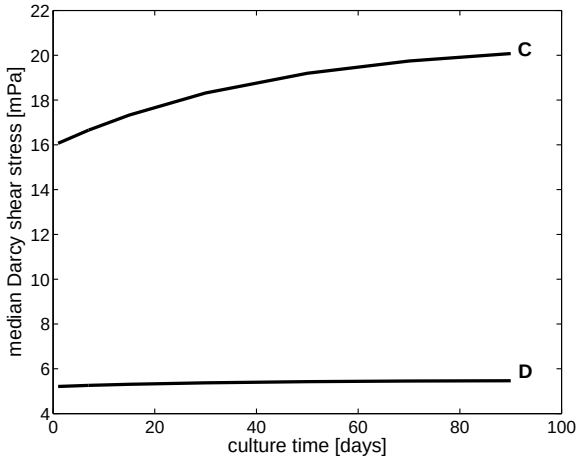

Figure 7: Median Darcy stresses as a function of culture time for different scaffold configurations and computed by using the PDE/ODE model described in Steps 1-4.

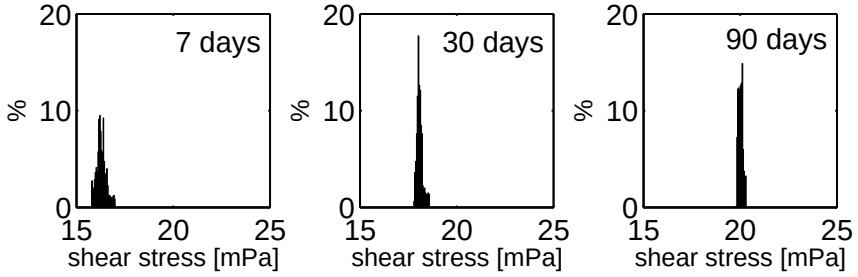

Figure 8: Shear stress distributions at different times of culture for scaffold C.

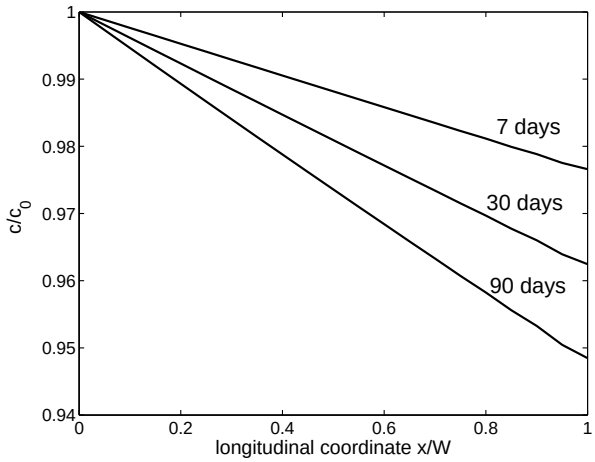

Figure 9: Oxygen concentration (normalized to the inlet concentration c_0) at different culture times computed by using the PDE/ODE model described in Steps 1-4. The x axis represents the dimensionless coordinate along the scaffold thickness.

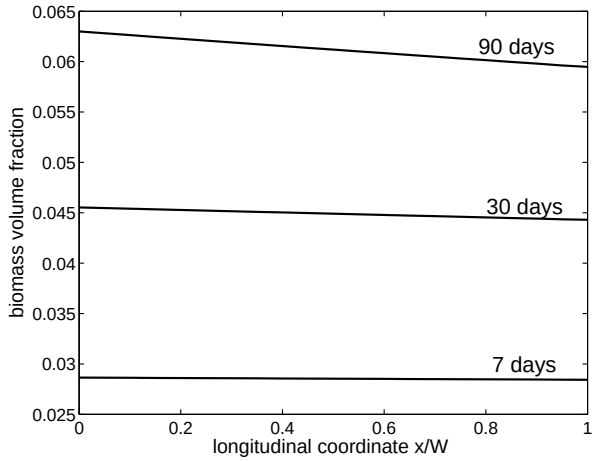

Figure 10: Average biomass volume fraction at different culture times computed by using the PDE/ODE model described in Steps 1-4. The x axis represents the dimensionless coordinate along the scaffold thickness.

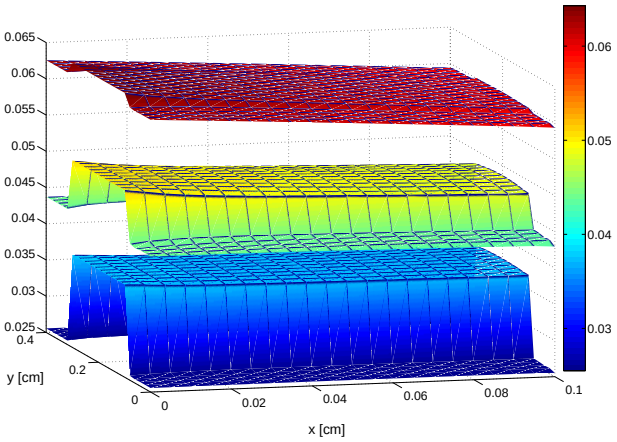

Figure 11: Spatial distribution of the biomass volume fraction at $t = 7, 30, 90$ days of culture (from bottom to top) under non–uniform seeding conditions. The seeding density in the inner region is 2 times greater than the seeding density in the uniform–seeding case.

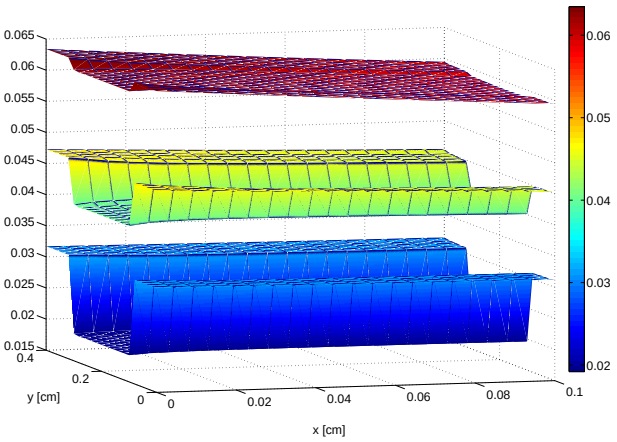

Figure 12: Spatial distribution of the biomass volume fraction at $t = 7, 30, 90$ days of culture (from bottom to top) under non–uniform seeding conditions. The seeding density in the inner region is 0.5 times lower than the seeding density in the uniform–seeding case.

MOX Technical Reports, last issues

Dipartimento di Matematica "F. Brioschi",
Politecnico di Milano, Via Bonardi 9 - 20133 Milano (Italy)

12/2010 Riccardo Sacco, Paola Causin, Paolo Zunino, Manuela T. Raimondi:
A multiphysics/multiscale numerical simulation of scaffold-based cartilage regeneration under interstitial perfusion in a bioreactor

11/2010 Paolo Biscari, Sara Minisini, Dario Pierotti, Gianmaria Verzini, Paolo Zunino:
Controlled release with finite dissolution rate

10/2010 Alfio Quarteroni, Ricardo Ruiz Baier:
Analysis of a finite volume element method for the Stokes problem

09/2010 Laura M. Sangalli, Piercesare Secchi, Simone Vantini, Valeria Vitelli:
Joint Clustering and Alignment of Functional Data: an Application to Vascular Geometries

08/2010 Francesca Ieva, Anna Maria Paganoni:
Multilevel models for clinical registers concerning STEMI patients in a complex urban reality: a statistical analysis of MOMI^2 survey

07/2010 Laura M. Sangalli, Piercesare Secchi, Simone Vantini, Valeria Vitelli:
Functional clustering and alignment methods with applications

06/2010 Jordi Alastruey, Tiziano Passerini, Luca Formaggia, Joaquim Peiró:
The effect of visco-elasticity and other physical properties on aortic and cerebral pulse waveforms: an analytical and numerical study

05/2010 Matteo Longoni, A.C.I. Malossi, Alfio Quarteroni, Andrea Villa:
A complete model for non-Newtonian sedimentary basins in presence of faults and compaction phenomena

04/2010 Marco Discacciati, Paola Gervasio, Alfio Quarteroni:
Heterogeneous mathematical models in fluid dynamics and associated solution algorithms

03/2010 P.E. Farrell, Stefano Micheletti, Simona Perotto:
A recovery-based error estimator for anisotropic mesh adaptation in CFD